Journal of Power Sources 262 (2014) 201–206

Contents lists available at ScienceDirect

Journal of Power Sources

journal homepage: www.elsevier.com/locate/jpowsour

Low cost preparation of Cu_2ZnSnS_4 and $Cu_2ZnSn(S_xSe_{1-x})_4$ from binary sulfide nanoparticles for solar cell application

Guilin Chen, Chenchen Yuan, Jiwan Liu, Yitao Deng, Guoshun Jiang, Weifeng Liu*, Changfei Zhu*

CAS Key Laboratory of Materials for Energy Conversion, Department of Materials Science and Engineering, University of Science and Technology of China, Hefei 230026, China

HIGHLIGHTS

- Solvent-free synthesis of binary sulfide nanoparticles for CZTS and CZTSSe thin films has been described.
- Cu, Zn, Sn sulfides nanoparticles are synthesized via a facile, solvent-free route, which is low cost and easy to scale-up.
- The influences of incorporation of sulfur/selenium on the CZTS/CZTSSe films have been investigated.

ARTICLE INFO

Article history:
Received 26 December 2013
Received in revised form
1 March 2014
Accepted 18 March 2014
Available online 26 March 2014

Keywords:
CZTS
CZTSSe thin films
Solvent-free synthesis
Annealing

ABSTRACT

A low-cost non-vacuum process for fabrication of Cu_2ZnSnS_4 (CZTS) and $Cu_2ZnSn(S_xSe_{1-x})_4$ (CZTSSe) films by solvent-free mechanochemical method and doctor blade process is described. First, CuS, ZnS and SnS nanoparticles are synthesized via a facile, solvent-free route, which is low cost and easy to scale-up. Second, the sulfides nanoparticulates precursors are deposited in a thin layer by doctor blade technique. Finally, the dry layers are sintered into CZTS/CZTSSe thin films. Different annealing processes are used, and the influences of incorporation of sulfur/selenium on the CZTS/CZTSSe films have been investigated. These structure, morphology and optical properties of CZTS/CZTSSe films are suitable for thin film solar cell fabrication.

1. Introduction

Photovoltaic solar energy conversion has the potential to fulfill increasing world energy consumption [1]. Most currently devices consist of silicon, which dominate the commercial market [2]. However, silicon is an absorber with indirect band gap, which necessitating a thick layer to absorb an appreciable fraction of the incident solar radiation. $CuIn_{1-x}Ga_xSe_2$ (CIGS) has been considered the most promising material for thin-film solar cells due to the direct band gap and high absorption coefficient (10^4–10^5 cm^{-1}), and the material utilization can be reduced to 1–2 um layer thickness [3,4]. However, this compound contains expensive materials such as In and Ga. Recently, Cu_2ZnSnS_4 (CZTS), $Cu_2ZnSnSe_4$ (CZTSe) and their solid solutions $Cu_2ZnSn(S_xSe_{1-x})_4$ (CZTSSe) have attracted significant attention owing to their interesting photoelectric properties [5,6]. As consisting of low-cost and readily available elements, they have high potential for mass production as solar absorber material [7,8]. Many groups focused on elaborating such materials in the past few years, using different methods including co-evaporation [9,10], sputtering [11], electroplating [12], nanoparticles [13,14], nanowire [15,16] and solution processing [17]. The latest report on CZTS and CZTSSe based devices have achieved promising efficiency of 8.4% and 12.6% by using a hydrazine based solution deposition technique [18,19]. However, the use of highly toxic and explosive hydrazine is considered to be a hurdle for commercial utilization. Another notable approach is nanoparticles-based method, Guo et al. have fabricated of 9.6% efficient CZTSSe thin films solar cell from binary/ternary sulfide nanocrystals [19]. They synthesized binary/ternary sulfide nanocrystals by hot injection technique. This method involves the injection of a cold solution of precursors into a hot surfactant solution (oleylamine) with an inert gas protection. The hot injection technique has drawbacks such as the complexity in process, production costs and difficulty in scaling up, which must be solved before the

* Corresponding authors. Tel.: +86 551 3600578; fax: +86 551 3601958.
E-mail addresses: liuwf@ustc.edu.cn (W. Liu), cfzhu@ustc.edu.cn (C. Zhu).

http://dx.doi.org/10.1016/j.jpowsour.2014.03.075
0378-7753/

commercialization of the CZTS solar cells [20]. On the other hand, the nanocrystals were capped with stabilizing molecules. The carbon generated from stabilizing molecules will prohibit crystal growth in the CZTS film during thermal treatment [21].

To explore the possibility of overcoming the above disadvantages, CZTS and CZTSSe thin films were prepared from binary sulfides nanocrystals. The binary sulfide nanoparticles were synthesized using a new, low-cost mechanochemical route at room temperature under atmosphere conditions. The approach is simple and cheap with the following advantages: (1) Normal atmosphere fabrication. No need to have inert gas protection; (2) Room-temperature synthesis. No need for heating; (3) Short reaction time. The whole synthesis process may only take up to several minutes; (4) Low cost and easy to scale-up to achieve ultra-large volume of sulfides binary; (5) The hot injection method is vulnerable to contamination by carbon from surfactant. Our binary sulfides ink was prepared by dispersed in ethanol without organic binder. The ethanol can evaporate quickly, thus residual carbon impurities may be minimized [20]. Meanwhile, the influence of annealing condition on the CZTS and CZTSSe films has been investigated.

2. Experimental

2.1. Preparation of binary sulfides nanoparticles and ink

Fig. 1 shows the flow diagram for CZTS and CZTSSe films fabrication. First, nano-sized CuS, ZnS, SnS powders were prepared by solvent-free mechanochemical method, respectively. In a typical synthesis, the metal chloride ($CuCl_2 \cdot 2H_2O$ or $ZnCl_2$ or $SnCl_4 \cdot 5H_2O$) and excess sodium sulfide were mixed thoroughly and ground with a mortar and pestle for several minutes. Then the as-milled powder was washed and filtrated, thoroughly dried at 60 °C to form the binary sulfide nanoparticles. Second, the obtained CuS, ZnS and SnS were weighed in stoichiometric ratios. Sequentially, the binary sulfides nanoparticles were dispersed in ethanol to form ink with concentration of 330 mg ml^{-1}.

2.2. CZTS and CZTSSe deposition processes

The binary sulfide precursors were deposited on the glass substrates in thin layers by doctor blade process. The precursor films were annealed under different conditions. For example, the annealing process was carried out without elemental sulfur/selenium either in vacuum (base $P \sim 10^{-1}$ Pa) or Ar ($P \sim 10^3$ Pa) (purity of Ar gas = 99.999%) at 550 °C for 30 min (referred to as Vacuum(V)-550 and Ar-550); with elemental sulfur/selenium in vacuum (base $P \sim 10^{-1}$ Pa) at 550 or 600 °C for 30 min (referred to as S-550, S-600, Se-550 and Se-600).

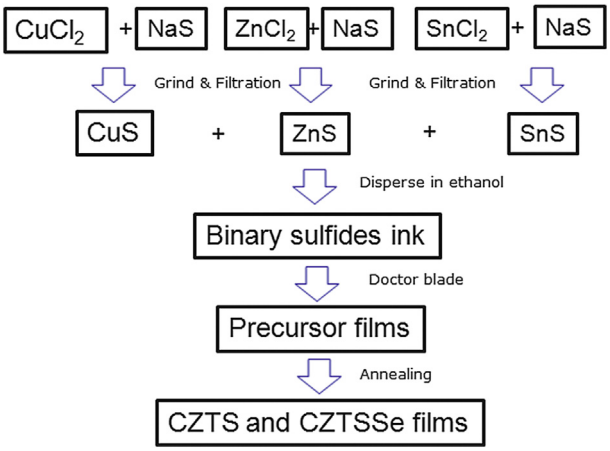

Fig. 1. Flow diagram for CZTS and CZTSSe films fabrication process.

2.3. Characterization

The phase composition and the crystal structure of the powders and films were identified by XRD method (D/Max-rA). The morphology of the film was observed on a field emission scanning electron microscope (FESEM, JEOL-JSM-6700F). The elemental composition of the film was determined by EDS measurements with a 20 acceleration voltage. The Raman measurements were performed at room temperature using a LABRAM-HR micro-Raman system in the back scatting configuration with a laser source of 514 nm. The X-ray photoelectron spectroscopy (XPS) spectra were carried out on thermo ESCALAB 250 spectrometer using an Al Ka monochromatized source and a multidetection analyzer under a 10^{-8} Pa residual pressure. The optical absorption spectrum was recorded on a UV–vis-365-type spectrophotometer in arrange 400–1200 nm.

3. Results and discussions

3.1. Preparation of binary sulfides nanoparticles

The solvent-free reaction is advantageous as it is induced at room temperature, and the synthesis time is very short, on the order of several minutes. In addition, this method requires no complex apparatus and techniques, and enables one to synthesize binary sulfides nanocrystals in high yields and at a large scale. The CuS, ZnS and SnS were prepared via a solvent-free solid–state reaction as follows:

$$Na_2S + MCl_2(M: Cu, Zn, Sn) \xrightarrow{Grind} MS + 2NaCl$$

The grinding is used to energize the reactant to make the reaction possible and accelerate solid state diffusion. So the reaction was observed to be very fast, the color of mixture changed quickly and remained black (CuS), white (ZnS) and brown (SnS) finally. Fig. 2 shows the XRD patterns of the resulting nanoparticles. All the X-ray peaks have been indexed, which confirmed the formation of CuS, ZnS and SnS nanoparticles. After milling of the mixture and subsequently washing, the CuS, ZnS and SnS phase appeared without any impurity phase, which indicated that the solid state

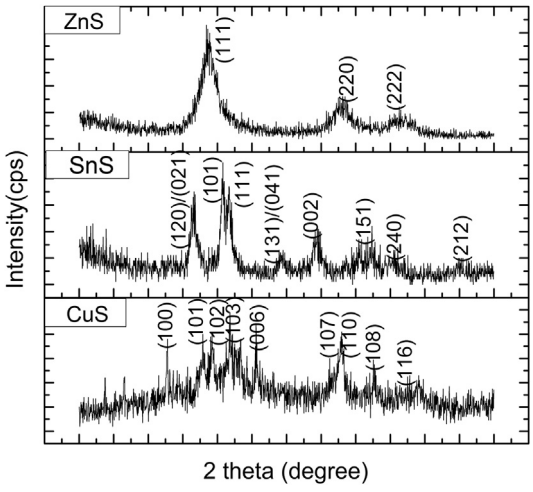

Fig. 2. XRD patterns of sulfide binary nanoparticles.

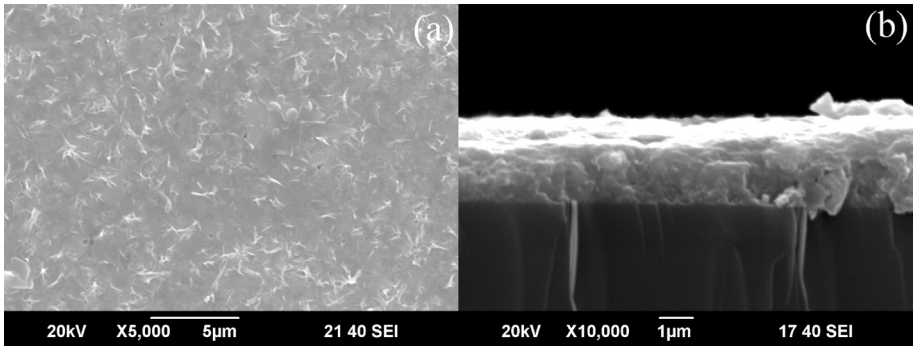

Fig. 3. Morphology and cross-section of precursor films.

reaction was complete. The average crystallite diameters of particles was calculated from the XRD data with Scherrer equation ($D = k\lambda/\beta \cos\ \theta$), where λ is the wavelength of the X-ray radiation, k is a constant taken as 0.89, θ is the diffraction angle, β is the full width at half maximum (FWHM) [22]. The crystallite diameters of CuS, ZnS and SnS were acquired by using CuS (103), ZnS(111) and SnS(101) peak. The FWHM were 0.326°, 0.597° and 0.447°, respectively. Finally, the calculated values of the crystal size of the nanocrystalline were about CuS: 25 nm, ZnS: 13 nm, SnS: 18 nm. So the solvent-free synthesis method is simpler and cheaper than other preparation methods, which can be applied in the CZTS and CZTSSe thin film for solar cell.

3.2. Precursor films

The precursor films were obtained after depositing the binary sulfide nanoparticles on the glass substrates. Fig. 3 shows the morphology and cross-sections of precursor film. It was observed that the binary sulfide particles were distributed uniformly. The precursor films are consisted of closely packed binary sulfide particles, which would be the key to grow the homogeneous and dense CZTS and CZTSSe films. As shown in Fig. 3(b), the thickness of the precursor films is about 1.7 um, with relatively smooth film surface.

3.3. Annealed layer

To obtain the CZTS and CZTSSe, the precursor was annealed under different atmosphere. The CZTS and CZTSSe film might be fabricated by reaction as follows:

$$2CuS + ZnS + SnS \xrightarrow{Annealing} Cu_2ZnSnS_4$$

$$2CuS + ZnS + SnS + S/Se \xrightarrow{Annealing} Cu_2ZnSnS_4 \text{ or } Cu_2ZnSn(S_XSe_{1-X})_4 + S/Se$$

Fig. 4(a) shows XRD patterns of the CZTS and CZTSSe thin films prepared under different annealing conditions. It revealed that the precursor films were nanocrystalline in nature. Upon heating under Vacuum, Ar or S-containing atmosphere, all films exhibit sharp diffraction peak (1 1 2), (2 0 0), (2 2 0) and (3 1 2). Moreover, the films exhibit the strongest peaks at (112) and (220) indicating a CZTS kesterite structure (JCPDS no. 26-0575) with a preferred grain orientation along (112). The result is in agreement with that obtained by Chen et al. [23]. As shown in the XRD, there were not obvious impurity phases in the synthesis. Compared with the above CZTS films, the main diffraction peaks of the selenized films were similar ($Cu_2ZnSnSe_4$, JCPDS no. 52-0868) but toward lower 2θ angle, which is attributed to the increased lattice space of larger Se atoms (0.198 nm) substitution of smaller S atoms (0.184 nm) [24]. However, the Cu_xSe was detected as a principal impurity phase.

In order to numerically characterize the crystallinity change, the full width at half maximum (FWHM) of (1 1 2) peaks of CZTS and CZTSSe films were calculated. Fig. 4(b) shows the FWHM of (1 1 2) peaks of CZTS and CZTSSe films prepared under various conditions. When the S/Se-containing atmosphere were used, the FWHM of (1 1 2) peaks decreased, indicating an increase in crystalline and grain size. It could be explained that under the S/Se-containing

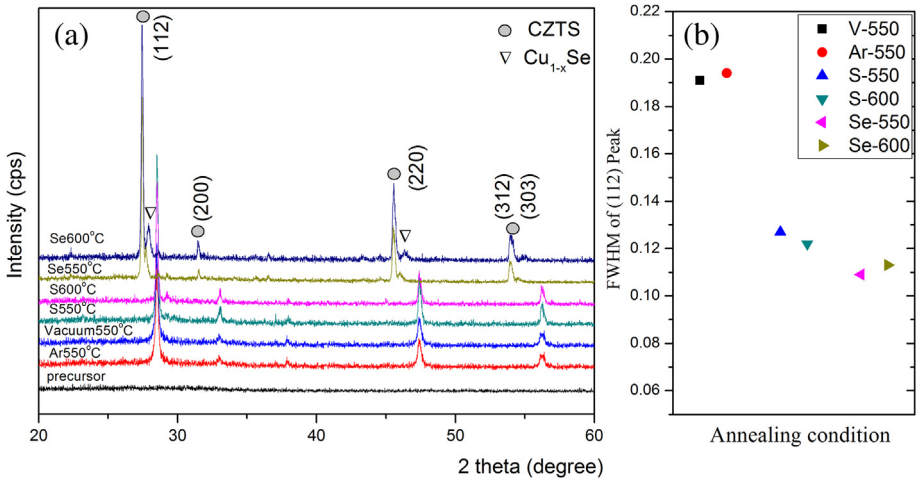

Fig. 4. XRD patterns of the (a) CZTS and CZTSSe thin films prepared under different annealing condition and (b) The FHWM for the (112) peak of films.

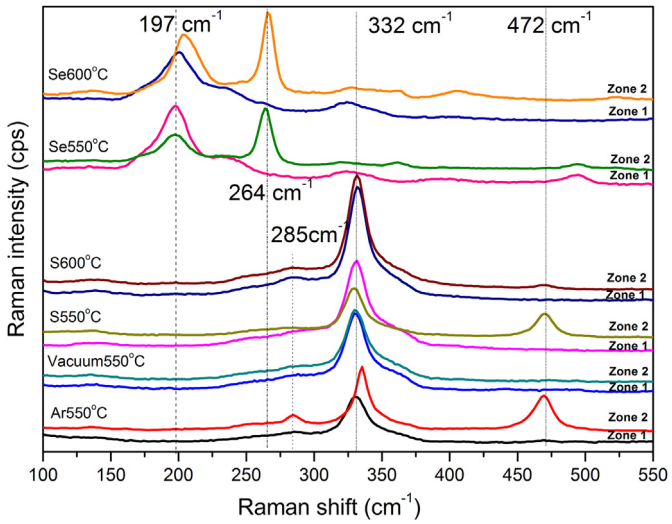

Fig. 5. Raman analysis of samples prepared under different condition in 2 different zones.

atmosphere, the diffusion of atoms, especially S/Se atoms, enhance significantly, resulting grain growth [25]. Therefore, the post annealing using sulfur/selenium vapor can be used to enhance the grain size of CZTS and CZTSSe films.

XRD is generally used as the main tool to analyze the structure, but XRD did not allow us to make a clear distinction between CZTS/CZTSSe and other possible secondary phase, such as Cu_2SnS_3, CuS, ZnS and Cu_2SnSe_3, CuSe, ZnSe. Raman scattering is a useful complimentary technique to identify secondary phase. According to literature [5,26], CZTS is known to have the following strong peaks: 285 and 333 cm^{-1}; ZnS: 352 and 275 cm^{-1}; Tetragonal Cu_2SnS_3: a big shoulder (280–290 cm^{-1}) and 297 cm^{-1}. Cubic Cu_2SnS_3: 267, 303 and 356 cm^{-1}. Orthorhombic Cu_2SnS_3: 318 cm^{-1}; SnS: 160, 190 and 219 cm^{-1} SnS_2: 314, 215 cm^{-1} Sn_2S_3: 52, 60 and 307 cm^{-1} Cu_2S: 264 and 475 cm^{-1}. CZTSe is known to have the following strong peaks: 174, 196 and 236 cm^{-1}; ZnSe: 205 and 252 cm^{-1}; $SnSe_2$: 186 cm^{-1}; CuSe at 264 cm^{-1}; Cu_2SnSe_3: 180, 236 and 251 cm^{-1}. Fig. 5 shows the results of Raman scattering in two zones of CZTS and CZTSSe films prepared under different conditions. After annealing, all the films exhibit CZTS or CZTSSe phases. Except Cu_2S and Cu_2Se phases, there are not any other secondary phases. The main peaks of the films (Vacuum-550, Ar-550, S-550, S-600) & (Se-550, Se-600) are marked: the peaks at around 285, 332 cm^{-1} are assigned to CZTS films [5]; the peaks at around 197 cm^{-1} are assigned to CZTSe films [27]. For Ar-550 and S-550 films, Zone 1 show a weak peak for $Cu_{2-x}S$ at 472 cm^{-1}, which is not observed in Zone 2. When using the higher sulfurization temperature (600 °C), the peak of $Cu_{2-x}S$ Raman modes disappears. So the higher sulfurization temperature can contribute to obtain pure CZTS phase. For selenized films, the existence of small peak (CZTS A1 mode: 332 cm^{-1}) indicate the formation of CZTSSe alloys.

Fig. 6 shows high resolution XPS spectra of the (a) Cu 2p, (b) Zn 2p, (c) Sn 3d and (d) Se 3d, Se3p & S2p core levels of the CZTS/Se thin films annealed under different annealing conditions. In Fig. 6(a), the peak of Cu 2p is split into 931.9 ($2p_{3/2}$) and 951.8 eV ($2p_{1/2}$) with a split orbit of 19.9 eV, corresponding to the Cu 2p core level in CZTS/Se [28]. The peak splitting with 19.8 eV has been

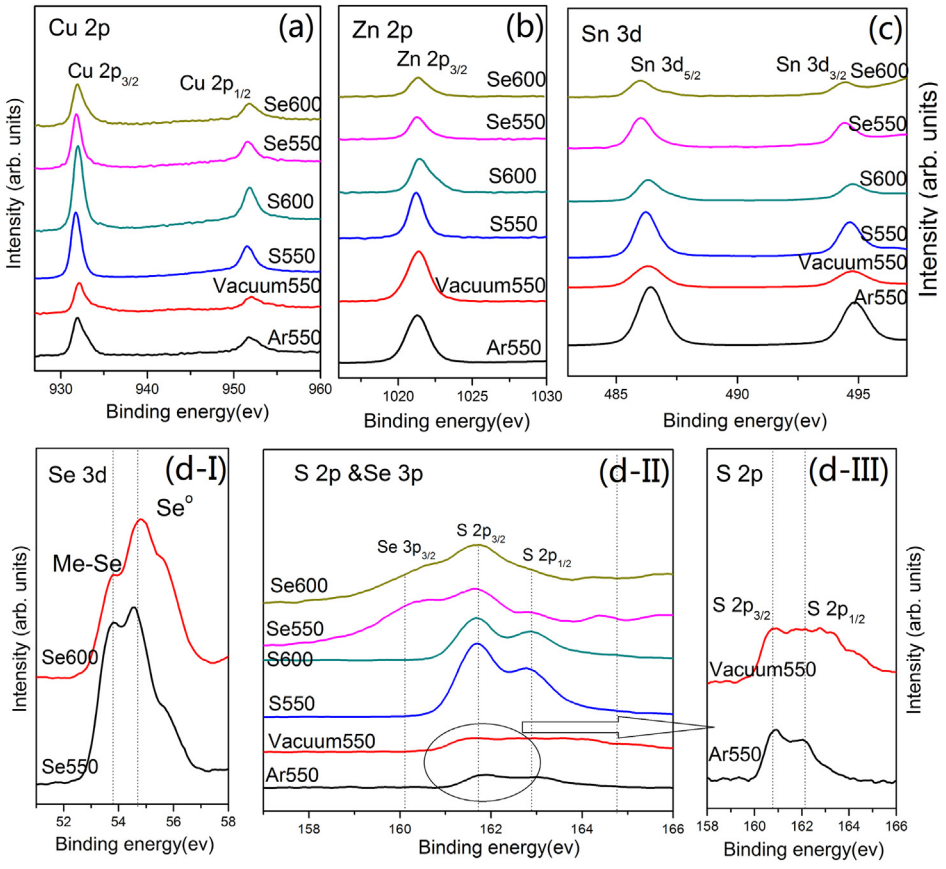

Fig. 6. XPS spectra of (a) Cu 2p, (b) Zn 2p, (c) Sn 3d and (d) Se 3d, Se3p & S2p core levels of CZTS/Se films.

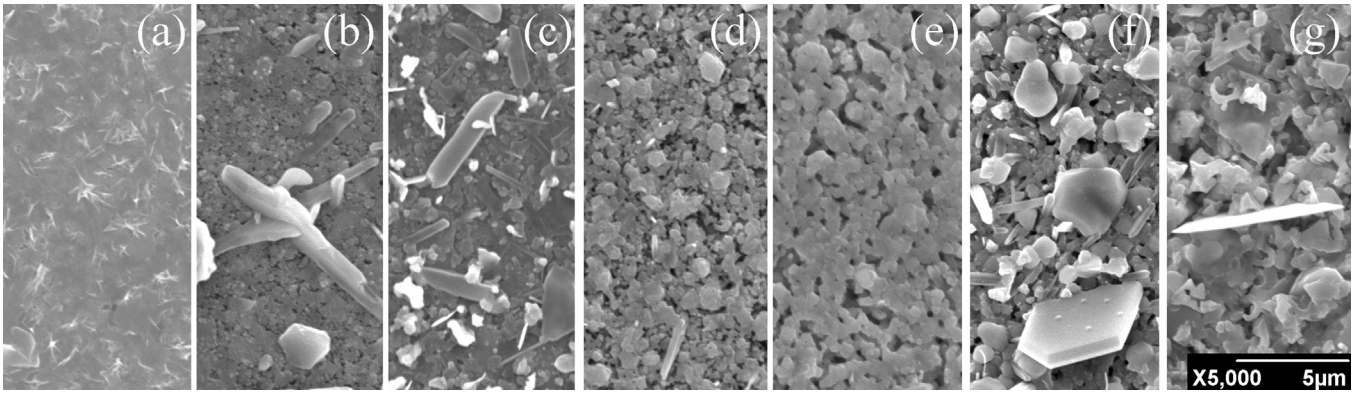

Fig. 7. SEM of the (a) precursor; CZTS thin films prepared under (b) Ar, (c) vacuum atmosphere, sulfurized at (d) 550 °C and (e) 600 °C; CZTSSe thin films selenized at (f) 550 °C and (g) 600 °C.

attributed to the Cu^{1+} ion, and there is no Cu $2p_{3/2}$ satellite peak located at about 942 eV for the contribution from Cu^{2+}. [29]. The binding energy at 1021.4 eV can be ascribed to the 2p electrons of Zn atoms (Fig. 6(b)), which are very similar to the previous report, suggesting that ZnS does not exist as a part of mixture and that the annealed films are CZTS/Se [16,30]. This behavior is consistent with the above XRD and Raman results. In Fig. 6(c), the peak of Sn 3d is split into 486.0 ($2p_{5/2}$) and 494.4 eV ($2p_{3/2}$) with a split orbit of 8.4 eV, which is in good accordance with the value of Sn(IV) [16]. As other valences such as Cu(II) and Sn(II) cannot be detected, it is not probably that Cu_3SnS_4 or Cu_3SnSe_4 coexists [4]. For all the CZTS, only the S 2p core-level spectrum is presented (Fig. 6(d-II)), the observed binding energy peaks located at 161.7 eV and 162.8 eV coincide with the electronic state of S $2p_{3/2}$ and S $2p_{1/2}$ core levels in the CZTS compound [5]. As the selenization was introduced, the selenium was incorporated. For Se-550 and Se-600 CZTSSe thin films, the Se 3d peak (Fig. 6(d-I)) located at 53.8 eV (Metal-Se) and 54.6 (Seo) eV, indicating Se^{2-} [23,31]. Simultaneously, the S 2p and Se 3p region were examined. This region consists of multi-peaks: 161.7 eV and 162.8 eV for S $2p_{3/2}$ and S $2p_{1/2}$; 160.1 eV for Se $3p_{3/2}$. The coexistence of Se and S indicated the formation of CZTSSe, which agreed with the Raman results.

Fig. 7 show SEM of the (a) precursor; CZTS thin films prepared under (b) Vacuum-550, (c) Ar-550, (d) S-550, (e) S-600, (f) Se-550 and (g) Se-600. It is clear that the Ar- & Vacuum-CZTS films are rough and nonuniform. The films exhibit a structure in that discrete large grains are spread around on the layer below, which itself composed of small grain. However, the surface became smooth and uniform and the grain improved greatly, when the films were subjected to anneal under sulfur atmosphere. Meanwhile, the larger grain has been found in the CZTS films prepared under higher temperature (600 °C) treatment. It was reported that a high temperature treatment of CZTS could results in increasing crystallinity and grain size [32]. The grain growth also occurs in the selenized films. But large surface roughness and some well-defined hexagon-shaped Cu_xSe were observed in the CZTSSe films, which agree well with XRD and Raman results. The impure phase Cu_xSe generally appears after selenization, which can be eliminated by KCN-etching [33]. It is well known that the efficiency of polycrystalline thin film solar cell increases with increasing grain size of the absorber layer [34]. From these above results, it is concluded that high temperature sulfurization/selenization is suitable to get CZTS and CZTSSe films with large grain from the binary sulfide, which could facilitate to fabricate high efficiency solar cells.

The elemental compositions deduced from EDS measurements are shown in Table 1. From composition analysis, it is found that there are some losses of Sn in CZTS/CZTSSe samples. It is probably due to the fact that Sn is easily lost by evaporation of SnS or SnSe phases at high annealing temperatures. Recent research found that the Sn losses can be alleviating by annealing under Sn, SnS or SnSe vapor atmosphere [35]. So in our future work, the addition of metallic Sn or $Sn(S,Se)_2$ will be carried out to control Sn losses. For the Se-550 and Se-600 thin films, S/(S + Se) ratios are determined to be 0.25, 0.15, respectively. This again confirms the formation of CZTSSe phase. Moreover, carbon which is a major undesirable contamination in solution or nanoparticles-processed solar cells

Table 1
Precursor film and annealed films composition measured by EDS.

	Cu (at.%)	Zn (at.%)	Sn (at.%)	S (at.%)	Se (at.%)	S/(S + Se)
Precursor	26.39	15.55	15.27	42.79	–	–
Ar-550	24.81	16.62	11.87	46.70	–	–
V-550	21.13	17.08	11.47	50.32	–	–
S-550	22.62	16.99	12.17	48.22	–	–
S-600	22.25	17.13	12.48	48.13	–	–
Se-550	21.59	21.24	10.92	11.84	34.40	0.25
Se-600	22.73	18.01	12.07	7.27	39.81	0.15

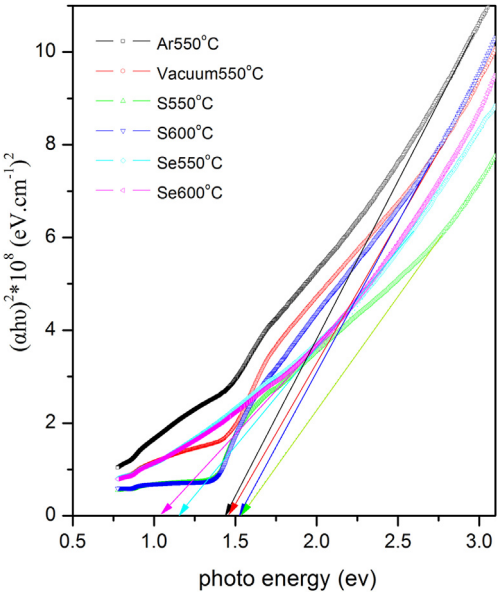

Fig. 8. The plot of $(\alpha h\upsilon)^2$ vs. $h\upsilon$ of CZTS and CZTSSe films prepared under different conditions.

was not detected in our CZTS/Se films. These data indicate that the ethanol can evaporate quickly, thus residual carbon impurities may be avoided.

Fig. 8. The plot of $(\alpha h\upsilon)^2$ vs. $h\upsilon$ of CZTS and CZTSSe films prepared under different conditions. Absorption study shows that the band gap energy of CZTS thin film is 1.44, 1.46, 1.53 and 1.52 eV for Ar, Vacuum, S-550, S-600 atm respectively; Whereas after selenization, it is found to be 1.16 and 1.03 eV for Se-550, Se-600 atm respectively. He et al. [36] have reported that the composition (S/(S + Se)) will affect the band gap of CZTSSe. So the band gap of CZTSSe was calculated in our study. According to the reference [36], the evolution of the Eg of CZTSSe solid solutions can be described as: $\mathrm{EgCZTSSe} = x\mathrm{EgCZTS} + (1-x)\mathrm{EgCZTSe} - bx(1-x)$. Where b is the optical bowing constant, the value of theoretical calculations is about 0.1 eV; and $x = \mathrm{S}/(\mathrm{S}+\mathrm{Se})$, which was calculated from the EDS results. So these determined Eg values of Se-550-CZTSSe ($x = 0.25$) and Se-6000-CZTSSe ($x = 0.15$) are 1.06, and 1.11 eV, respectively. Our experimental data for the band gap of CZTSSe are consistent with the calculated results. Those observed optical energy band gap is quite close to that of previous report, which can be applied as the absorb layer of thin film solar cell [16,26].

4. Conclusion

In summary, we have successfully demonstrated the synthesis of CuS, ZnS, SnS nanoparticles in an easy and low cost solvent-free reaction. After coating the ink including binary sulfide precursors and annealing, the CZTS and CZTSSe films were obtained in our work. Comparative study between post annealing using Ar, Vacuum, sulfur vapor and selenium vapor was carried out to optimize the CZTS and CZTSSe film. The diffusion of sulfur/selenium in the film during the annealing process can improve the crystallinity and morphology of the film. As a result of this study, it indicates a promising low cost way for the application in CZTS and CZTSSe thin film solar cells.

Acknowledgment

This work was supported by National Basic Research Program of China (973 Program)-2012CB922001, the Fundamental Research Funds for the Central Universities and the Fundamental Research Funds for the Central Universities (WK2060140005).

References

[1] D.B. Mitzi, O. Gunawan, T.K. Todorov, K. Wang, S. Guha, Sol. Energy. Mater. Sol. Cells 95 (2011) 1421–1436.
[2] M.A. Green, J. Mater. Sci. Mater. Electron 18 (2007) 15–19.
[3] M. Kemell, M. Ritala, M. Leskela, Crit. Rev. Solid State Mater. Sci. 30 (2005) 1–31.
[4] H.W. Schock, Prog. Photovolt.: Res. Appl. 160 (2000) 151–160.
[5] L.J. Chen, Y.J. Chuang, J. Power Sources 241 (2013) 259–265.
[6] C. Wadia, A.P. Alivisatos, D.M. Kammen, Environ. Sci. Technol. 43 (2009) 2072–2077.
[7] T.M. Friedlmeier, H. Dittrich, H.W. Schock, in: The 11th Conference on Ternary and Multinary Compounds, ICTMC-11, Salford, 8–12 September 1997, pp. 345–348.
[8] L.J. Chen, J.D. Liao, Y.J. Chuang, CrystEngCommun 13 (2011) 2909–2914.
[9] I. Repins, C. Beall, N. Vora, C. DeHart, D. Kuciauskas, P.T. Dippo, B. Toa, J. Mann, W.C. Hsu, A. Goodrich, R. Noufi, Sol. Energy. Mater. Sol. Cells 101 (2012) 154–159.
[10] B. Shin, O. Gunawan, Y. Zhu, N.A. Bojarczuk, S. Jay Chey, S. Guha, Prog. Photovolt: Res. Appl. 21 (2013) 72–76.
[11] J. Han, S.W. Shin, M.G. Gang, J.H. Kim, J.Y. Lee, Nanotechnology 24 (2012) 095706–095708.
[12] L. Guo, Y. Zhu, O. Gunawan, T. Gokmen, V.R. Deline, S. Ahmed, L.T. Romankiw, H. Deligiann, Prog. Photovolt: Res. Appl. (2012), http://dx.doi.org/10.1002/pip.2332.
[13] Q. Guo, G.M. Ford, W.C. Yang, B.C. Walker, E.A. Stach, H.W. Hillhouse, R. Agrawal, J. Am. Chem. Soc. 132 (2010) 17384–17386.
[14] A. Shavel, J. Arbiol, An. Cabot, J. Am. Chem. Soc. 132 (2010) 4514–4515.
[15] L. Shi, C. Pei, Y.g Xu, Q. Li, J. Am. Chem. Soc. 133 (2011) 10328–10331.
[16] L.J. Chen, Y.J. Chuang, J. Cryst. Growth 376 (2013) 11–16.
[17] D. Aaron R. Barkhouse, O. Gunawan, T. Gokmen, Teodor K. Todorov, D.B. Mitzi, Prog. Photovolt: Res. Appl. 20 (2012) 6–11.
[18] W. Wang, M.T. Winkler, O. Gunawan, T. Gokmen, T.K. Todorov, Y. Zhu, D. B. Mitzi, Adv. Energy Mater, http://dx.doi.org/10.1002/aenm.201301465.
[19] Q. Guo, Y. Cao, J.V. Caspar, W.E. Farneth, A.S. Ionkin, L.K. Johnson, M. Lu, I. Malajovich, D. Radu, K.R. Choudhury, H.D. Rosenfeld, W. Wu, in: Photovoltaic Specialists Conference (PVSC), 2012 38th IEEE, 3–8 June 2012, pp. 002993–002996.
[20] K. Woo, Y. Kim, J. Moon, Energy Environ. Sci. 5 (2012) 5340–5345.
[21] O. Zaberca, F. Oftinger, J.Y. Chane-Ching, L. Datas, A. Lafond, P. Puech, A. Balocchi, D. Lagarde, X. Marie, Nanotechnology 23 (2012) 185402–185413.
[22] A.W. Burton, K. Ong, T. Rea, Y.C. Ignatius, Microporous Mesoporous Mater. 117 (2009) 75–90.
[23] L.J. Chen, Y.J. Chuang, Mater. Lett. 91 (2013) 372–375.
[24] Y. Sun, K. Zong, H. Zheng, H. Wang, J. Liu, H. Yan, M. Zhu, Mater. Lett. 92 (2013) 195–197.
[25] W.M. Hlaing Oo, J.L. Johnson, A. Bhatia, E.A. Lund, M.M. Nowell, M.A. Scarpulla, J. Electron. Mater. 40 (2011) 2214–2221.
[26] L. Shi, Q. Li, CrystEngComm 13 (2011) 6507–6510.
[27] G. Chen, W. Liu, G. Jiang, B. Pan, C. Zhu, Sol. Energy 92 (2013) 172–175.
[28] S.W. Shin, S.M. Pawar, C.Y. Park, J.H. Yun, J. Moon, J.H. Kim, J.Y. Lee, Sol. Energy. Mat. Sol. Cells 95 (2011) 3202–3206.
[29] G.L. Chen, W.L. Liu, G.S. Jiang, J. Li, C.F. Zhu, J. Alloys Compd. 531 (2012) 91–95.
[30] S.S. Mali, B.M. Patil, C.A. Betty, P.N. Bhosale, Y.W. Oh, S.R. Jadkar, R.S. Devan, Y. Ma, Electrochim. Acta 66 (2012) 216–221.
[31] M. Danilson, M. Altosaar, M. Kauk, A. Katerski, J. Krustok, J. Raudoja, Thin Solid Films 519 (2011) 7407–7411.
[32] N. Nakayama, K. Ito, Appl. Surf. Sci. 92 (1996) 171–175.
[33] W. Witte, R. Kniese, M. Powalla, Thin Solid Films 517 (2008) 867–869.
[34] K. Tanaka, N. Moritake, H. Uchiki, Sol. Energy Mater. Sol. Cells 91 (2007) 1199–1201.
[35] A. Redinger, D.M. Berg, P.J. Dale, S. Siebentritt, J. Am. Chem. Soc. 33 (2011) 3320–3323.
[36] J. He, L. Sun, S. Chen, Y. Chen, P. Yang, J. Chu, J. Alloys Compd. 511 (2012) 129–132.